Smart Structures and Systems, *Vol. 27, No. 2 (2021) 227-239*
DOI: https://doi.org/10.12989/sss.2021.27.2.227

Implementation of video motion magnification technique for non-contact operational modal analysis of light poles

Jothi S. Thiyagarajan [1a], Dionysius M. Siringoringo[*2], Samten Wangchuk [3b] and Yozo Fujino [2c]

[1] *School of Infrastructure, Indian Institute of Technology Bhubaneswar, Odisha 752050, India*
[2] *Institute of Advanced Sciences, Yokohama National University, Yokohama 240-8501, Japan*
[3] *Department of Urban Innovation, Yokohama National University, Yokohama 240-8501, Japan*

(*Received July 13, 2020, Revised October 20, 2020, Accepted October 23, 2020*)

Abstract. Damages on lights and utility poles mounted on the elevated highway or railway bridges were observed in the past several large earthquakes. The damages could have serious consequences to public safety, travelling vehicles or trains, and nearby properties. A previous study shows that the damages were caused by buckling and yielding of the pole due to excessive response amplification during large earthquake. Such amplification occurs when the bridge's natural frequency is close to the light pole's fundamental frequency. An investigation of the seismic performance of existing light pole mounted on elevated highway bridges is needed to avoid the response amplification. This includes the identification of the light pole's natural frequency and damping ratio. Vibration testing of the light pole using conventional contact sensors individually would require enormous effort and is time-consuming. Moreover, such vibration testing on a highway bridge deck would require traffic disruption to provide access. Video camera-based non-contact vision sensing is seen as a promising alternative to the conventional contact sensors for this purpose. The objective of this paper is to explore the use of non-contact vision sensing for operational modal analysis of light pole on highway viaduct. The phase-based video motion magnification method is implemented to obtain the light pole response in an ambient condition. Using this method, small and invisible displacement is magnified for a certain range of frequency of interest. Based on the magnified video frames, structural displacement is extracted using the image processing technique. The natural frequency and damping ratio of the light pole are estimated using the random decrement technique. The method is verified in a laboratory-scale experiment and implemented to practical field measurements of a light pole on a highway viaduct in Kanagawa, Japan. The results are compared with measurement by Laser Doppler Vibrometer. Both experiments suggest that the method could effectively obtain the natural frequency and damping ratio of the structures under the ambient condition where vibration amplitudes are very small and invisible with reasonable accuracy.

Keywords: computer vision; motion magnification; operational modal analysis; light pole; vibration measurement

1. Introduction

Failures of light poles, utility poles, and transmission poles on highway or railway bridge networks have been reported in some of the past large earthquakes in Japan (Siringoringo *et al*. 2020). The failures have serious consequences to public safety, travelling vehicles or trains, and nearby properties. Secondary effects such as disruption of power supply, industrial production, and rescue and recovery operations in the earthquake-affected areas could also follow. As a secondary structural member, light poles mounted on highway bridge may be subjected to severe problems as their vibrations are directly influenced by bridge vibration in addition to external excitation sources. Previous studies show that the damages were caused by buckling and yielding of the pole due to excessive response amplification during large earthquake (Izuno *et al*. 2008, Siringoringo *et al*. 2020). Such amplification occurs when the bridge's natural frequency is within a close range of the light pole's fundamental frequency. An investigation of the seismic performance of existing light pole mounted on elevated highway bridges is needed to avoid the response amplification. This includes estimating the natural frequency and damping ratio of existing light poles via operational modal analysis (OMA).

OMA is commonly used to estimate the modal properties of large infrastructures like bridges and buildings in their operational condition when they are subjected to various input force excitations like traffic, wind, and other dynamic loads. Various techniques for extracting modal parameters from the operational condition have been available and implemented in numerous studies (Brincker and Ventura 2015, Wenzel 2009, Peeters and De Roeck 2001, Siringoringo and Fujino 2008). The common approach is to use vibration response of the structures such as acceleration, velocity, or displacement obtained under unknown input conditions. The structure responses were obtained by various types of vibration sensors, which can be broadly categorized as contact and non-contact sensors.

*Corresponding author, Ph.D., Associate Professor,
E-mail: dion@ynu.ac.jp
[a] Formerly Postdoctoral Researcher,
E-mail: tjs@iitbbs.ac.in
[b] E-mail: samten-wangchuk-gs@ynu.jp
[c] E-mail: fujino-yozo-bv@ynu.ac.jp

ISSN: 1738-1584 (Print), 1738-1991 (Online)

Contact sensors like contact accelerometers (wired or wireless) are attached to the structural members. However, the conventional measurement by contact sensors has numerous limitations, such as mass loading effect, and low spatial and temporal resolution due to single point measurement. Conventional measurement of existing light poles individually by contact sensors would require enormous effort and is time-consuming. Moreover, such vibration testing on a highway bridge deck is often difficult without traffic disruption to provide personnel access.

A non-contact vibration measurement system can provide higher spatial resolution measurements and added consistent information. Many non-contact measurement methods like speckle pattern interferometry and holographic interferometry (Pedrini *et al*. 2006), laser scanning vibrometer (Siringoringo and Fujino 2006, 2009), multi-object tracking algorithm (Ye *et al*. 2016a), and GPS with wavelet filtering techniques (Ni *et al*. 2019) have been developed in the past. These measurement systems, however, are relatively expensive for massive usage. It is desirable to achieve high measurement resolution by alternative non-contact measurement methods through digital high-speed video cameras, which are relatively less expensive and easy to set up (Helfrick *et al*. 2011).

Recently, computer vision has been used extensively for structural health monitoring of civil infrastructure (Feng and Feng 2018). The use ranges from dynamic response measurement to damage detection. With available image processing algorithms, full-field modal information can be obtained successfully from video camera-based measurements with surface preparation like speckle pattern or high-contrast reflection markers. Such vision sensors are relatively easy and agile to set up and provide significantly more high-spatial-density measurements where any pixel could become a measurement point.

Advanced computer vision algorithms like phase-based video motion magnification techniques have been successfully developed to effectively process large-scale image/video data for extracting detailed structural dynamic information under small amplitude motion. Phase-based video motion magnification technique has been proposed for OMA (Wadhwa *et al*. 2013, Chen *et al*. 2015, Ye *et al*. 2016b, Chen *et al*. 2017, Poozesh *et al*. 2017, Yang *et al*. 2017, 2018, Sarrafi *et al*. 2018, Molina-Viedma *et al*. 2018, Chen *et al*. 2018). Various computer vision-based signal processing and machine learning techniques like edge detection, principal component analysis, blind source separation, etc., are utilized (Yang *et al*. 2019, 2020, Bhowmick and Nagarajaiah 2020). These developments have been investigated and verified in laboratory-scale experiments, and some have been implemented for full-scale modal analysis of structures.

In this paper, the implementation of phase-based video motion magnification technique for non-contact OMA of existing light poles on highway viaduct is described. The paper is organized such that the basics of the phase-based video motion magnification technique are firstly explained. This is followed by description on displacement extraction method from the magnified video motion. Then, experiment verification is provided to demonstrate the feasibility of the displacement extraction method and modal parameters estimation. Finally, the method is implemented to practical field measurements using a video camera for modal identification and vibration measurements of existing light pole-viaduct systems.

2. Methodologies

In this study, the procedure for OMA of the light pole using video measurement consists of three main steps: (1) phase-based video motion magnification, (2) displacement extraction from video, and (3) modal analysis, as shown schematically by Fig. 1. Each step comprises detailed processes and techniques described in this section. The theoretical background on the methodologies is explained concisely in this section to provide a general idea of the methods and how they were implemented in the study. Interested readers are recommended to find a detailed explanation of each method from the main references.

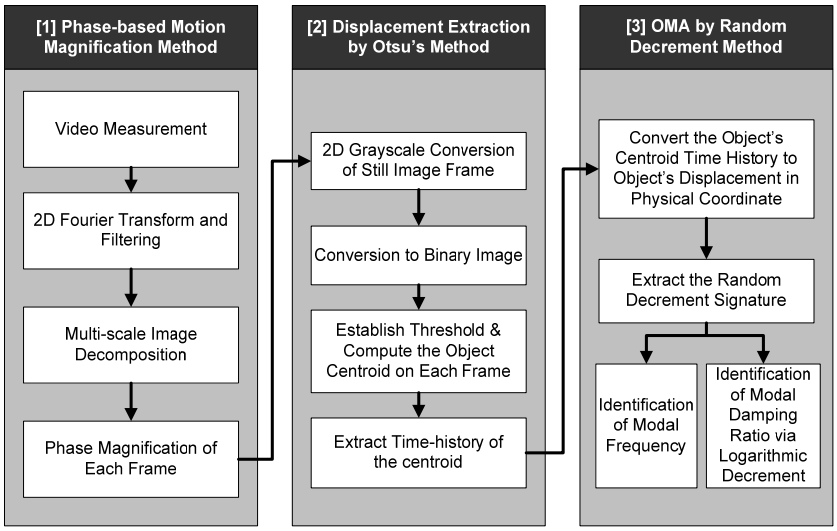

Fig. 1 Flowchart of the procedure for OMA using phase-based motion magnification technique

2.1 Local phase-based vibration motion magnification method

Video measurement of structural vibration contains temporally displaced frames with image intensity, $I(x+\delta(x,t))$ where x is the pixel coordinate, and $\delta(x,t)$ is the spatially and temporally varying local motion. The captured video motion can be determined by its magnitude and local phase using two-dimensional Fast Fourier Transform (2D-FFT), and it is extracted by multi-scale and localized filters. Notably, the phase information conveys a better estimate of the motion than magnitude (amplitude) as it is unaffected by illumination effects and surface conditions. We closely follow the work by Wadhwa *et al.* (2013) for the methodology, and for completeness, we add important equations that are described in this section.

The basic principle of the local phase-based motion magnification technique is that in a particular frequency band, the video obtained is the magnified version of the original one, obtained by frequency-bandpass filtering, amplifying and reconstructing the signals from the original video. The phase-based motion magnification algorithm decomposes a video's signal into the local spatial amplitude and phase using a complex-valued steerable pyramid filter bank. The local spatial phase signals are temporally Fourier decomposed into a series of sinusoids representing harmonic motion. The phase signals are then temporally bandpass filtered, amplified, and recombined to form a motion magnified video. As explained by Wadhwa *et al.* (2013), each frame (subset) in a video (set) is spatially multi-scale and temporally local, $\delta(x,t)$, and it is required to extract the local phase. The complex steerable pyramid filters, which are complex Gabor filters with sinusoids windowed by a Gaussian envelope, leading to finite spatial support, are applied to extract local amplitudes and local phases (Portilla and Simoncelli 2000). By Fourier series decomposition, the displaced frames can be represented as a sum of complex sinusoids (Eq. (1)), in which each band corresponds to single-frequency ω.

$$I\big(x+\delta(x,t)\big)=\sum_{\omega=-\infty}^{\infty}P_{\omega}e^{i2\pi\omega(x+\delta(x,t))} \tag{1}$$

$$B_{\omega}(x,t)=P_{\omega}e^{i2\pi\omega(x+\delta(x,t))} \tag{2}$$

where $B_{\omega}(x,t)$ are a sinusoid subband representation and its phase $\omega(x+\delta(x,t))$ contains motion information. Similar to the Fourier shift theorem, the motion can be manipulated by altering the phase. To isolate motion in specific temporal frequencies, the phase-in Eq. (2), $\omega(x+\delta(x,t))$ is temporally filtered and then multiply the band passed phase with magnification factor α as $I\big(x+(1+\alpha)\delta(x,t)\big)$, which magnifies the phase of the particular subband $B_{\omega}(x,t)$.

$$\tilde{B}_{\omega}(x,t)=B_{\omega}(x,t)e^{i\alpha2\pi\omega\delta(x,t)}=P_{\omega}e^{i2\pi\omega(x+(1+\alpha)\delta(x,t))} \tag{3}$$

The resulting $\tilde{B}_{\omega}(x,t)$ is a complex sinusoid, and it has $(1+\alpha)$ times magnified input motion. Thus, the phases of each coefficient are magnified by this amount for each frame. The pyramid type considered is half octave bandwidth. The motion magnified video can be reconstructed by collapsing the pyramid. After computing spatial filters, one can calculate the phase differences from the reference frame for each level. Then, necessary temporal bandpass filtering is applied before introducing the amplification factor (α). As α is introduced, noise characteristics in the image get translated rather than magnified. For a particular scale and orientation, the response for a noisy image $I+\sigma_n n$.

$$N_{\omega}=B_{\omega}(x,t)+\sigma_n M_{\omega}(x,t) \tag{4}$$

where $M_{\omega}(x,t)$ is the response of n to the complex steerable pyramid filter indexed with ω. Because of magnification, the response is shifted by $e^{i\alpha2\pi\omega\delta(x,t)}$. Thus, the motion magnified band is represented as

$$\widetilde{N}_{\omega}(x,t)=\tilde{B}_{\omega}(x,t)+\sigma_n e^{i\alpha2\pi\omega\delta(x,t)}M_{\omega}(x,t) \tag{5}$$

When the pyramid is collapsed, this phase shift corresponds to a translation of the noise. However, the input sequence noise may add the noise to the phase, resulting in incorrect magnification. Thus, the amplitude-weighted spatial Gaussian blur on the phases is introduced. For each frame k and each band i, it has a phase $\varphi_{i,k}$ and amplitude $P_{i,k}$. Thus, a weighted Gaussian blur is computed as

$$\big(\varphi_{i,k}P_{i,k}\big)*K_{\rho}/P_{i,k}*K_{\rho} \tag{6}$$

where K_{ρ} is a Gaussian kernel. A 2-D Gaussian smoothing kernel with standard deviation specified by sigma (σ) is utilized. It returns a rotationally symmetric Gaussian lowpass filter. Lastly, combine all the phase magnified frames to form a final video, which allows us to see small motions without noise.

2.2 Displacement extraction by Otsu Threshold Segmentation Method (OTSM)

The image processing technique for tracking the displacement of the structural members from the magnified video is implemented to extract the modal frequencies of the structure. The displacement extraction algorithm can be independently used on various cropped regions of the video to extract the structure's displacement in those regions. The cropped regions are considered a virtual sensor, giving the displacement signal for that structure's location. The phase magnified video is represented as a four-dimensional (4D) array as, a-by-b-by-3-by-k and it is divided into k separate frames of a still image. The real color images are converted to grayscale by eliminating the hue and saturation information while retaining the luminance. By using Otsu Threshold Segmentation method (OTSM) (Otsu 1979), the object's characteristic on the frames of a still image is defined and using the continuous frames of the still image; one can trace the movement of the object. The main idea of OTSM is described in this section.

Consider the pixels of a given frame of still image represented in L gray levels $[1,2,\dots L]$. The number of

pixels at level i is denoted by n_i, and the total number of pixels by $N = n_1, n_2, +\ldots n_L$. The gray-level histogram is normalized and regarded as a probability distribution

$$p_i = \frac{n_i}{N}, \qquad p_i \geq 0, \qquad \sum_{i=1}^{L} p_i = 1 \tag{7}$$

As suggested by Otsu (1979), the pixels can be divided into two classes C_0 and C_1 (background and objects, or vice versa) by a threshold at level k. In light pole still image, this can be done quite easily by taking a video sky as a background. The C_0 denotes pixels with levels [1, 2.., k], and C_1 denotes pixels with levels $[k+1, \ldots L]$. A criterion that measures the separability of a threshold at level k can be defined as the function of probabilities of class occurrence, and the class means levels as follows.

$$\eta(k) = \sigma_B^2(k) \,/\sigma_T^2 \tag{8}$$

where

$$\sigma_B^2(k) = \frac{[\mu_T \omega(k) - \mu(k)]^2}{\omega(k)[1-\omega(k)]} \tag{9}$$

$$\sigma_T^2(k) = \sum_{i=1}^{L} (i - \mu_T)^2 p_i \tag{10}$$

The quantities $\omega(k)$ and $\mu(k)$ are the probabilities of class occurrence and class means, respectively.

In the implementation of the method, 2D grayscale images are utilized to create binary images by replacing all values above a globally determined threshold with ones and setting all other values to zeros by choosing the threshold value defined in the above equations to minimize the intra-class variance of the threshold black and white pixels. To compute the threshold, a 256-bin image histogram is employed. Finally, the center of the mass of a region (centroid) is calculated for both x and y direction in the pixel resolution. The centroid of mass for each frame at a specific time is denoted as the location of the object. Therefore, by collecting centroid information of the object from continuous time frames, one can obtain the object's displacement as a function of time. This plot represents the displacement extraction of the structure in the time domain.

2.3 Extraction of modal parameters from displacement response

The procedure to extract modal parameters from structural responses is an essential step in the OMA. Numerous methods have been developed in the literature from which one can select the most appropriate condition. To identify the modal parameters of a light pole, several key conditions need to be considered. First, a light pole vibration is typically dominated by the first flexural mode, which means that without loss of generality, the modal identification can be treated as a single-degree-of-freedom (SDOF) modal identification problem aiming at a modal frequency and damping identification. Second, the adoption of the SDOF identification problem is suitable since the displacement response is obtained from the centroid of rigid body motion per frame, as explained in the previous section. Third, the extracted displacement response is a random structural response under unknown excitation. Considering the three conditions above, the random decrement technique for modal frequency and damping estimation of the random response of the SDOF system is adopted in this study. Note that for other cases where the structure is flexible, and the vibration cannot be defined solely by the SDOF system, other displacement extraction procedures and modal identification should be considered.

The random decrement technique is a fast and simple technique to obtain a random decrement signature from a random response by simple time averaging (Cole 1973, Ibrahim 1977). The random decrement signature has been proved to correspond to the correlation function (Vandiver *et al*. 1982) from which the modal parameters commonly obtained from free vibration response can be extracted.

Given the $y(t)$ is a random displacement time history, the random decrement signature response $x(\tau)$ is obtained after averaging N sets of time histories with equal time length τ.

$$x(\tau) = \frac{1}{N} \sum_{i=1}^{N} y(t_i + \tau) | C_{y(t_i)} \tag{11}$$

where the random responses $y(t)$ at time steps $t_i = t_1, t_2 \ldots t_N$ satisfy the triggering condition $C_{y(t_i)}$. The constant level needs to be maintained to avoid averaging the deterministic part, giving the free-decay step response. This is achieved by setting the triggering condition from which the sample of timestamps of random responses is selected. Normally, a level of crossing $y(t_i) = C_a$, where C_a is the fraction of root means square (RMS) of random response is selected as the triggering condition (Siringoringo and Fujino 2008). In this study, $C_a = 0.8$ is selected as the triggering condition. The random decrement signature response also allows for estimation of damping employing logarithmic decrement (δ) as expressed below

$$\delta = \frac{1}{n} ln \frac{x(t)}{x(t+nT)} \tag{12}$$

from which the modal damping ratio (ζ) is calculated

$$\zeta = \frac{1}{\sqrt{1 + (\frac{2\pi}{\delta})^2}} \tag{13}$$

Note that δ is the natural log of the ratio of the amplitudes of any two successive peaks. $x(t)$ and $x(t + nT)$ are the vibration amplitudes at time t and $t + nT$ of the decaying vibration or the random decrement signature, respectively, and n is an integer number of successive, positive peaks.

3. Experimental verification

3.1 Experimental verification on cantilever beam

In order to validate the phase-based motion magnification algorithm, displacement extraction technique, and random decrement method, firstly, experimental verification

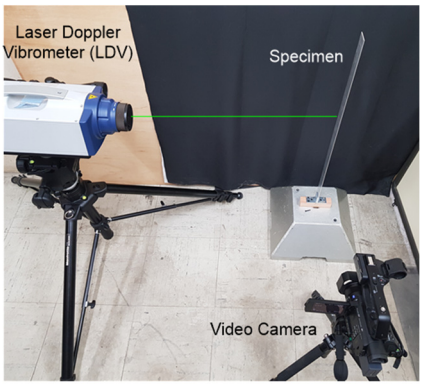

(a) Setup for cantilever beam experiment with LDV as reference

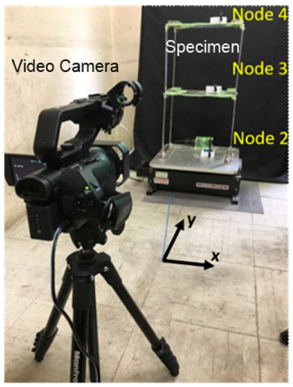

(b) Setup for an experiment using a two-story shear frame model using wireless accelerometers as reference

Fig. 2 Experimental verification by a high-speed video camera system

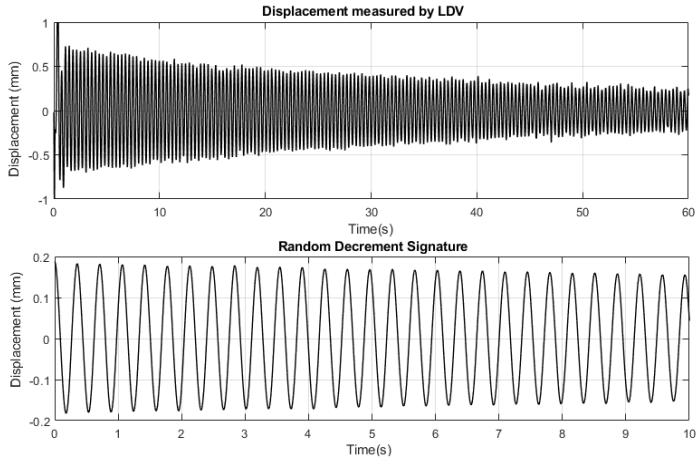

(a) Displacement and random decrement signature

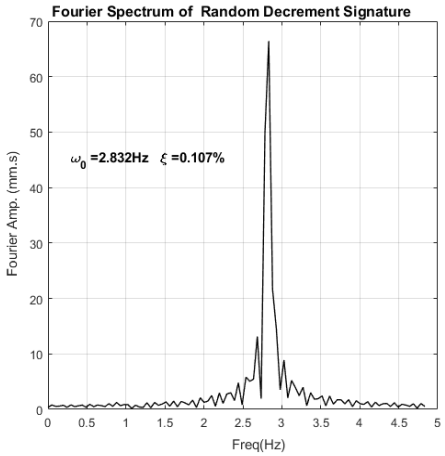

(b) Fourier amplitude spectra of random decrement signature

Fig. 3 Displacement response of the cantilever beam measured by LDV

was conducted on a cantilever beam specimen. The specimen is selected to model the light pole. The cantilever is made of aluminum with dimension: height 750 mm, width 40mm, and thickness 2 mm. The beam is fixed on the bottom to simulate cantilever support. The cantilever vibration is measured on its weak axis only. Laser doppler vibrometer (LDV) Polytec's RSV-150 is placed on the same vibration direction plane, and the laser beam is directed perpendicularly towards the structure displacement. Responses from LDV are utilized to verify the measurement results obtained by a video camera.

To record the motion of the specimen, a high-speed stationary video camera (SONY NXCAM with pixel resolution 2160 × 1080) mounted with the Zeiss lens was used. The camera captures a full field video measurement of the structure with the frame rate set to 30 fps. The ordinary indoor lighting was provided without any external illumination enhancement condition. The verification test setup is shown in Fig. 2. The specimen was excited by introducing a small deformation on the top of the plate to initiate the free vibration response. The first theoretical modal frequency of the cantilever plate on its weak axis can be calculated using the formula $\omega_{01} = \frac{1.875^2}{2\pi}\sqrt{\frac{EI}{\rho L^4}}$; where Young's modulus of the aluminum specimen was E = 69 GPa. This gives a frequency of 2.903 Hz.

Fig. 3(a) shows the free vibration responses obtained by laser doppler vibrometer, the random decrement signature, and Fourier spectra of random decrement signature. The results show that, the cantilever plate vibration is dominated by the first mode and identified at 2.832 Hz, which slightly lower than the theoretical value but still within a reasonable range of estimation. The damping ratio of the first mode is estimated to be 0.107% by the random decrement method.

The video measurement was captured simultaneously, and it was post-processed by applying the phase-based magnification technique for the selected frequency band. The pixel resolution of the video for further processing is downsampled at 1358 × 864 × 1824, where 1824 represents the number of frames sampled at the frequency 30 Hz. The magnified frames are kept separated for implementing the proposed displacement extraction technique, as shown in Fig. 4. The true-color image is converted to a grayscale image and binary image, which is utilized to compute the

(a) Frame of magnified motion (b) Converted grayscale image (c) Converted binary image

Fig. 4 Temporal frame (frame 140th) of magnified motion of the cantilever beam model

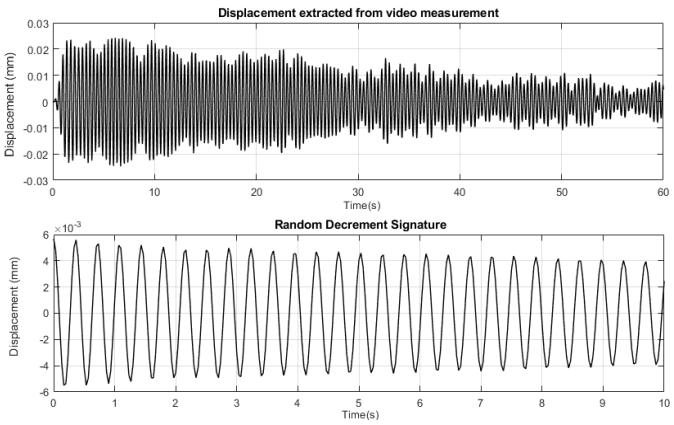

(a) Displacement and random decrement signature

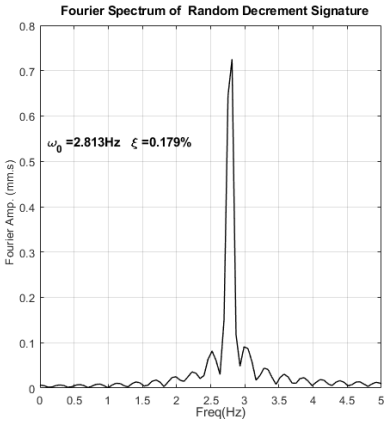

(b) Fourier amplitude spectra of random decrement signature

Fig. 5 Displacement response of the cantilever beam extracted from a video camera

center of mass of the region (centroid) in pixel resolution. The pixel coordinate is converted to displacement domain as a function of time in the weak axis direction, as shown in Fig. 5. The first set of post-processing is done for the magnifying phase in the cut off frequency range of 2.5 – 3 Hz as the first modal frequency lies within this range, as shown in Fig. 5(a), and the amplification factor, α is kept as 100. The amplitude of the displacement is in the range of ±0.05 mm, which is a small invisible motion.

It should be noted that the displacement time history of LDV and the one obtained from video measurement is not the same. This is because the displacement time-history obtained from video measurement is derived from the centroid of binary still image using Otsu's method. Because of cropping and sizing, this centroid may not be located at the same location as the LDV measurement point. Nevertheless, both time-histories should contain the same modal information of vibration (i.e., natural frequency and damping) because they were measured from the same vibration object.

Random decrement signature from the extracted displacement was computed, as shown in Fig. 5(b). Afterward, the random decrement techniques were applied to obtain the natural frequency and damping ratio. The estimated natural frequency was 2.813 Hz, and the damping ratio was 0.179%. The identified natural frequency is in good agreement with the result of vibration measurement by LDV. The damping ratio, although slightly higher, is still within reasonably good agreement with the LDV result.

3.2 Experimental verification two-story shear frame model

The second experiment was conducted on a two-story shear frame model to simulate a two-degree of freedom model. The model is made of aluminum columns with its base fixed to a base frame and lumped weights added to plates on both the floors of the model (Fig. 2(b)). The free vibration test is carried out by exciting the structure horizontally (x-direction) on the top floor. This means that

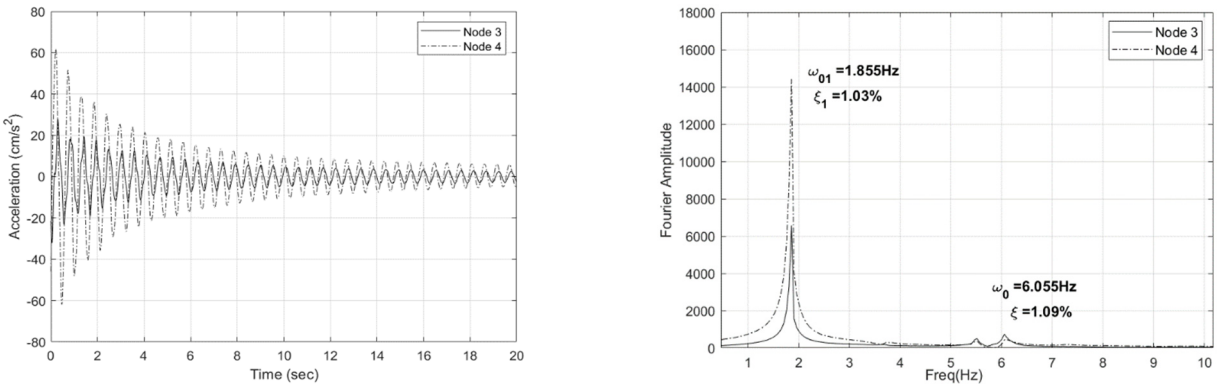

(a) Free vibration response (b) Fourier spectra of free vibration response

Fig. 6 Accelerations of two-story shear frame model in x-direction measured by wireless sensors

(a) Still frame of magnified motion (b) Converted grayscale image (c) Converted binary image

Fig. 7 Temporal frame (570th frame) of the 2DOF shear building frame model

the structure vibrates mostly in the x-direction. Three triaxial wireless accelerometer sensors are attached on each floor to measure acceleration (Ground – Node 2, Floor 1- Node 3, and Floor 2 – Node 4). Note that in this experiment, the LDV was not used because it can only measure the response from a single contact point, while in this case, two measurement points were needed. The sampling frequency for the wireless sensor is 100 Hz. The measured acceleration by Node 3 and Node 4 wireless sensors along with its Fourier Spectra Amplitude (FSA) are shown in Figs. 6(a) and (b), respectively. Note that although the wireless sensors are triaxial, only the x-direction of response is considered in the analysis. The structure is excited horizontally in the x-direction, and the major response of structure as can be captured by the video camera is also in the x-direction. The first two modal frequencies are obtained as 1.855 Hz and 6.055 Hz, and the corresponding damping ratios are 1.03% and 1.09%, respectively. These modal parameters will be used as reference values.

Like in the first experiment, we used the high-speed stationary video camera (SONY NXCAM with pixel resolution 2160 × 1080) to capture the structure's full field video measurement at the frame rate of 30 fps. The video measurement was captured at an ambient condition where the vibration was very small and almost invisible. Afterward, the video was post-processed by applying the phase-based magnification technique for the selected frequency band. The pixel resolution of the video was downsampled to 1358 × 864 × 570, where 570 represents the number of frames, and the sampling frequency was selected as 30 Hz. The magnified frames were kept separated for implementing the proposed displacement extraction technique.

Fig. 7 shows an example of a process for one frame of a still image. The true-color image was converted to a grayscale image and binary image, which was utilized later to compute the center of mass of the region (centroid) in pixel resolution. The pixel coordinate was converted to the displacement domain as a function of time, as shown in Fig. 8. The first set of post-processing was conducted for the magnifying phase in the cut off frequency range of 1.8 – 2 Hz as the first modal frequency lies within this range (1.85 Hz), as shown in Fig. 8(a), and the amplification factor, α is kept as 100. The amplitude of the displacement is in the range of ±0.5 mm, which is a small invisible motion. The extracted center of mass of the region (centroid) in pixel coordinate is converted to the displacement domain as a function of time.

Using random displacement responses extracted by the motion magnification method, a random signature response was calculated. The modal frequency was identified at

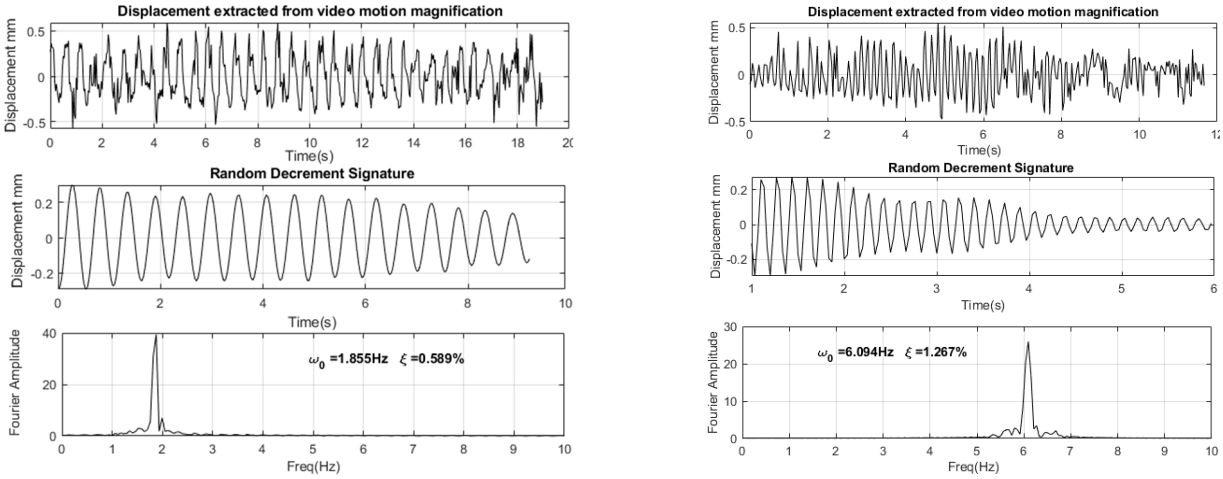

(a) First mode (b) Second mode

Fig. 8 Displacement of the two-story shear frame model extracted from video using motion magnification method, random decrement signature, and spectra of random decrement signature

1.855 Hz, which is in good agreement with the value obtained from vibration measured by acceleration. The damping ratio was identified at 0.589%, lower than the damping value obtained from acceleration. Similarly, the entire process was repeated for magnifying the phase of the motion in the cut off frequency range of 6-6.2 Hz for attaining the second modal frequency. The displacement extracted from the video is plotted in Fig. 8(b). The random signature response was calculated from the displacement, and the modal frequency was identified 6.09 Hz, which agrees well with the value obtained from vibration measured by acceleration. The damping ratio was identified at 1.267%, slightly higher than the damping value obtained from acceleration but still within a reasonable range of estimation.

Both experimental verification cases demonstrate that modal frequency estimation results by video motion using phase-based motion magnification agree well with reference values measured by conventional vibration sensors (i.e., laser doppler vibrometer and wireless accelerometers). However, the damping ratio estimation has lower consistency and accuracy, which can be attributed to the difficulty in estimating damping from random decrement technique for a relatively short displacement response.

It should be mentioned that image processing requires extensive computer computation, depending on the pixel size of the frame. For example, the calculation time for a 1-minute video with pixel resolution 2160 × 1080 and frame rate 30 fps is about four hours at the PC with the processor-Intel(R) Core(TM) i7-8650U, CPU1.90 GHz 2.11 GHz, and 16 GB RAM of memory. The heavy computation sometimes limits the attainable length of displacement response extracted from video measurement.

(a) Light poles considered for vibration measurement (b) Experimental setup with LDV and high-speed video camera system

Fig. 9 Field experiment on a light pole-viaduct system at two different locations

4. Full-scale implementation

The proposed method was implemented on the field measurement to obtain the vibration response of the light pole-viaduct system under ambient conditions. The structural system selected for the measurement is the light pole on top of the highway bridge at the Kinko JCT, Kanagawa, Japan. It is a three-part continuous double-deck elevated bridge consisting of two double-deck curved bridges and one single-deck parallel straight bridge. The curved bridges have a length of 185 m and 240 m with curve radii 91.9 m and 72 m, respectively. Four light poles were selected as the measurement objects, as shown in Fig. 9(a). The light pole is a tall type pole named STB9.1 with a total height of 9.1 m. The pole's diameter is 139.8 mm at the bottom and tapered to 89.1 mm in the middle to the top with a width of 60.5 mm. The bottom of the pole is fixed on a base steel plate with the size 35 cm × 40 cm and anchored to the highway curb by M30 high tension bolts. The base plate and pole are connected by welding with four U-shaped rib plates. Each pole weighs about 130 kg and is made of carbon steel pipe STK 400 with a modulus of elasticity 206000 N/mm^2. These light poles are manufactured by the same company and fixed using the same technique but located at different parts of the bridge. It should be mentioned that signboards with the weight 15.2-26 kg were attached to some of the light poles. The verification study is conducted to investigate the possible variation of the light pole modal parameter.

For reference, a laser Doppler vibrometer (Polytec's RSV-150) was utilized to measure the vibration of the pole. The LDV can provide a non-contact, highly accurate vibration measurement at a distance of more than 30m, a typical distance between the poles and the measurement devices in this experiment. The light pole motions were captured high-speed video camera system SONY NXCAM with pixel resolution 2160 × 1080. The measurement was carried out simultaneously using LDV for displacement measurement and a video camera capturing the structure's ambient motion. Both devices measured the target light pole from the same location, as shown in Fig. 9(b). The measurement is made in an outdoor setting with uncontrolled lighting and without any controlled active excitation of the structure.

4.1 Results of measurement by LDV

Note that the light pole vibration can be divided into in-plane and out-of-plane vibration. The vibration direction that coincides with the lamp's hook is considered the main or strong axis' vibration, named the in-plane vibration. Meanwhile, the vibration direction perpendicular to the strong axis is considered as the weak axis or out-of-plane vibration. Based on the light pole's design drawing, it was confirmed that geometry and material are very similar along with the pole's height in strong and weak axis except for the mass attached near the top that represents the lamp and signboard. Thus, normally the light pole fundamental frequencies in the strong and weak axis are very close (Siringoringo *et al*. 2020). The measurement using LDV was conducted by pointing the laser toward the middle point of the pole and arranging such that the light pole's out of plane vibration was mostly recorded.

Fig. 10 shows the displacement response obtained from LDV for poles P-1 and P-2, respectively. These are the light poles without signboards. The plot illustrates the original detrended signal, the random decrement signatures, and their respective Fourier spectra amplitude. Measurement results show that the pole's vibration is dominated by the fundamental mode, which is the first mode in the out-of-plane direction. This mode was identified at 1.563 Hz and 1.611 Hz for P1 and P2, respectively. The modal damping ratios for these modes were estimated by random decrement as 0.18% and 0.15%, respectively. The values signify the

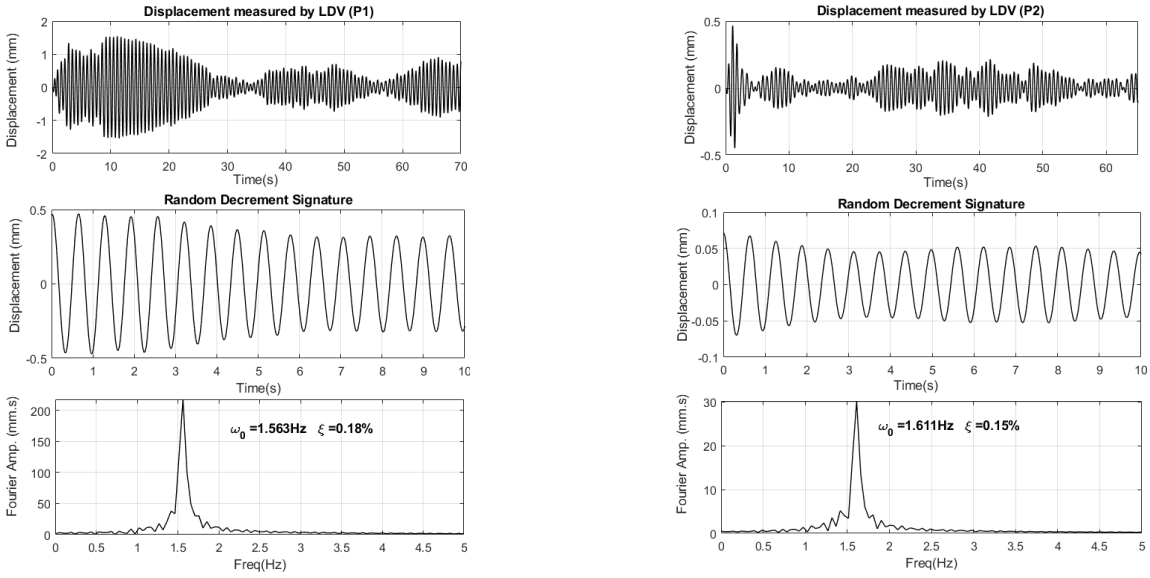

(a) Light pole P1 (b) Light pole P2

Fig. 10 Displacement measured by LDV, random decrement signature and spectra of random decrement signature of the light poles without signboard

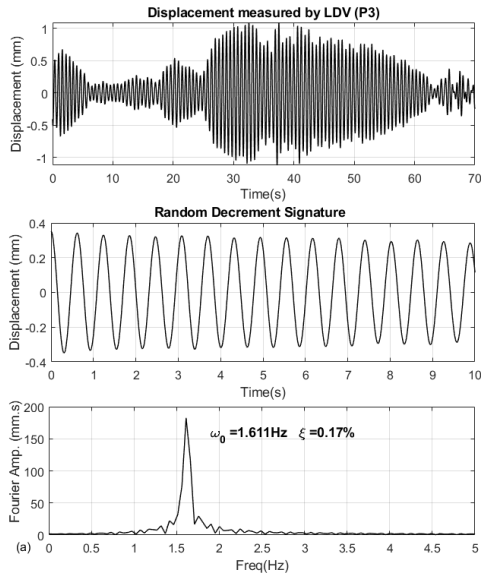

(a) Light pole P1

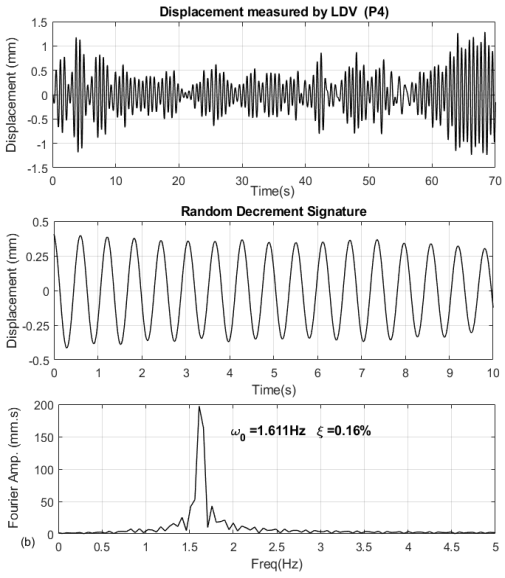

(b) Light pole P2

Fig. 11 Displacement measured by LDV, random decrement signature and spectra of random decrement signature of the light poles with signboard

low damping of the pole, consistent with the results of experimental modal analyses using accelerometers conducted previously on similar light poles (Siringoringo *et al*. 2020).

Results of measurement for light poles P3 and P4 are shown in Fig. 11. These poles have a signboard attached to the main body. The first modal frequency of both poles obtained by the random decrement method was equal at 1.61 Hz; whereas the modal damping ratios obtained by the logarithmic decrement method are 0.16% and 0.17% for pole P3 and P4, respectively. The estimated modal parameters of all light poles from LDV measurements are listed in Table 1.

4.2 Results of measurement by video camera and phase-based motion magnification

The video camera is placed on the footpath about a distance of over 75 m from the target structure. The video recording was carried out at a frame rate of 30 fps with a pixel resolution of 2160 × 1080. The original videos were downsampled for further analysis. For example, the down-sampled video of pole P1 is at 1268 × 1268 × 3600-pixel resolution, while 3600 represents the number of frames. The phase-based motion magnification technique was implemented for temporal frames of the light pole head section. The cut-off frequency range was fixed at 1.4-1.7 Hz as the modal frequency value of light pole obtained through LDV measurement lies within this range, as illustrated in Table 1. The amplification factor α was set at 100, and the sampling frequency was 30 Hz.

In Fig. 12, the temporal frames from a magnified video (e.g., 1120th -1190th) sampled at ten frames interval obtained from the pole P3 are shown as an example. The figure shows the evolution of pole motion amid after 100 times magnification suggesting very small original motion. The motion magnified frames are utilized to trace the displacement of the structure. The pixel resolution for the downsampled video is 219 × 219 × 1950. The magnified motion of temporal frames are converted to grayscale images and followed by constructing the binary images using OTSM for computing the displacement of the structure, as shown in Fig. 13. From each frame of a still image, the binary image and the center of mass (centroid) is

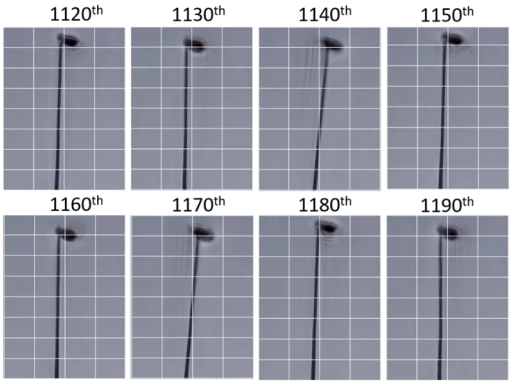

Fig. 12 Temporal frames from a magnified video showing the small motion of the light pole P3

Table 1 Comparison results of extracted modal parameters from LDV and vision-based measurements

Light pole attachment / ID		Random decrement method			
		LDV		Vision-based	
		Frequency (Hz)	Damping ratio	Frequency (Hz)	Damping ratio
Without sign board	P-1	1.563	0.180	1.523	0.110
	P-2	1.611	0.150	1.640	0.250
With sign board	P-3	1.611	0.170	1.611	0.196
	P-4	1.611	0.160	1.641	0.125

(a) Downsampled temporal frame (b) Converted grayscale (c) Binary images

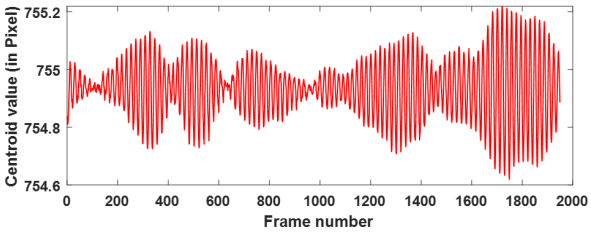

(d) The centroid value per frame.

Fig. 13 Example of the process from video measurement until the estimation of centroid location of the still image of 1200th temporal frame of light pole head (P2)

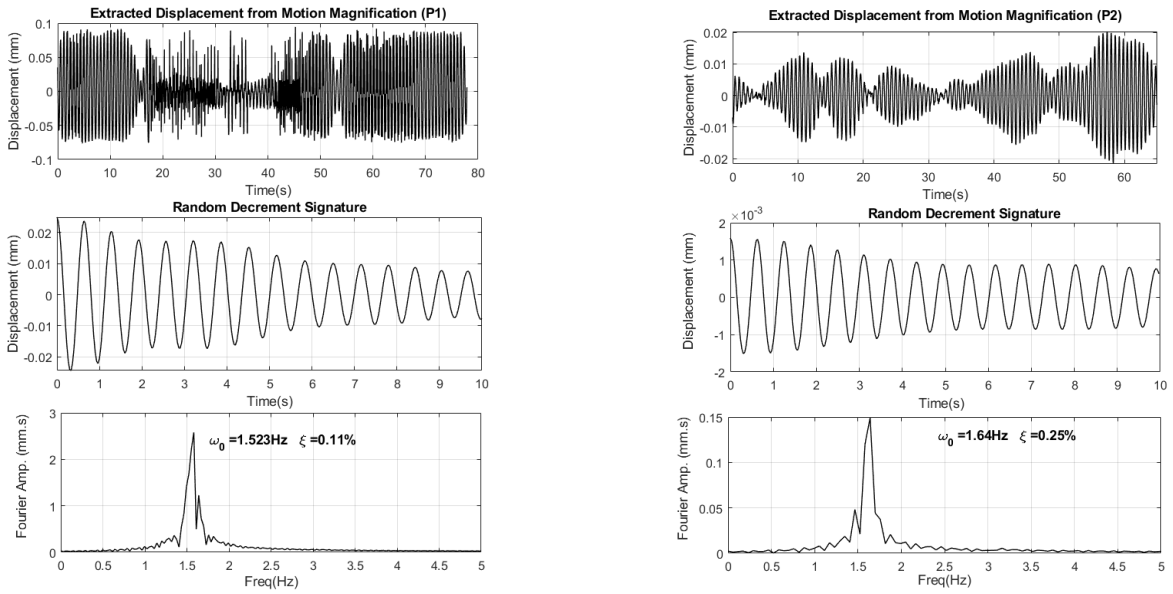

(a) Light pole P1 (b) Light pole P2

Fig. 14 Displacement measured by phase-based motion magnification method, random decrement signature, and spectra of random decrement signature of the light poles without a signboard

computed. An example of the centroid value in pixel value of all frames is illustrated by Fig. 13(d) for P2. The displacement is obtained by transforming the pixel coordinate system to physical displacement system in time domain.

Fig. 14 shows the displacement response obtained from a video-based motion magnification method for poles without signboard attached, P1 and P2, respectively. The plot illustrates the extracted displacement responses, the random decrement signatures obtained by applying the random decrement technique to the extracted displacement responses, and the Fourier spectra of the random decrement signature. By applying the random decrement analysis, the identified natural frequencies were 1.523 Hz and 1.64 Hz, for P1 and P2, respectively. In comparison, the damping ratios for both poles were estimated by random decrement as 0.11% and 0.25% for P1 and P2, respectively. These values, although slightly different from the LDV results, are generally still in good agreement. A similar procedure was implemented to video measurement of poles P3 and P4. The results are illustrated in Fig. 15. The identified natural frequencies were 1.611 Hz and 1.641 Hz, and the corresponding damping ratios were 0.196% and 0.125% for P3 and P4, respectively. The extracted modal parameters are tabulated in Table 1 to compare all the attained results. Compared to the modal frequencies, it is observed that the values are generally in very good agreement with the reference LDV data. Whereas the damping ratio values

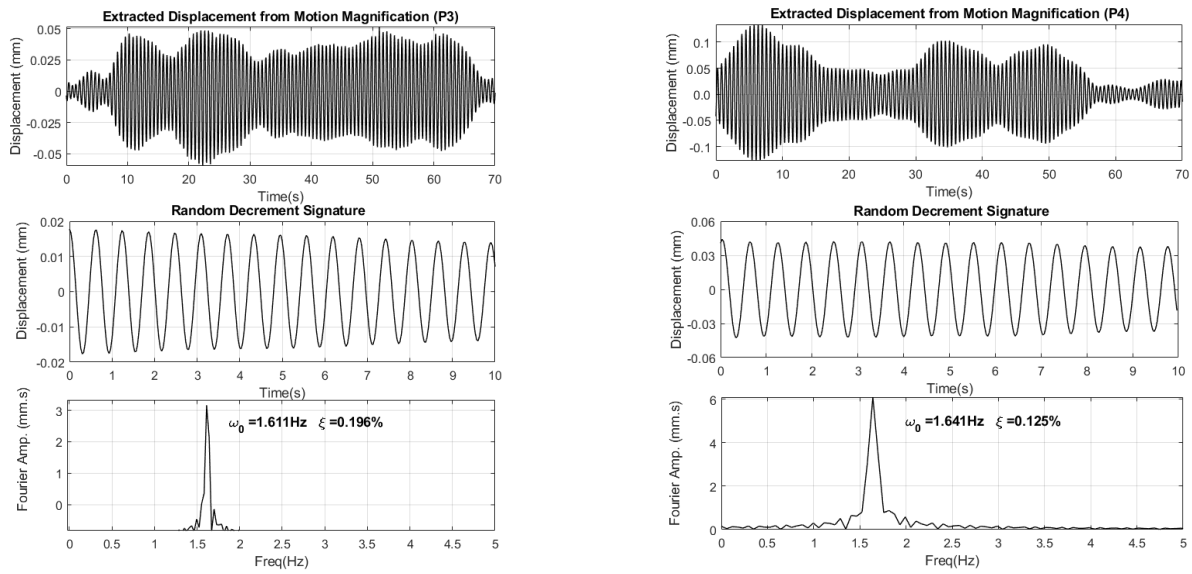

(a) Light pole P3 (b) Light pole P4

Fig. 15 Displacement measured by phase-based motion magnification method, random decrement signature, and spectra of random decrement signature of the light poles with a signboard

obtained from a vision-based response are slightly different but still within the reasonable range.

The previous study showed that 90% of the structural vibration is captured by the first fundamental natural frequency. Hence, only the first mode frequency is considered in this research. Vibration of the typical light pole investigated was characterized by fundamental in-plane and out-of-plane mode with low structural damping with a damping ratio of 0.1–0.2%. With these dynamic characteristics, the damping ratio results through LDV and vision-based vibration measurement of the light pole are between the range of 0.11-0.25% (Table 1), which shows good agreement with the previous study.

5. Conclusions

This paper describes a study on the implementation of a phase-based video motion magnification technique for OMA of light poles. The phase-based motion magnification technique is based on phase manipulation of motion and tracking the spatiotemporal frame displacements. Displacement of the light pole is extracted from the frames of an image using centroid-based Otsu threshold segmentation method. Modal parameters of the light pole are identified from displacement response using the random decrement technique. The image processing technique is promising in representing displacement (both in-plane and out-of-plane vibration) of the structures since only the first mode frequency is considered in the research. Experimental verifications were conducted using a cantilever beam and two-story shear frame models. The results demonstrated that the techniques can effectively identify modal parameters of the structures with reasonable accuracy.

The full-scale implementation of the method was conducted to identify the modal parameters of the light poles on the highway viaduct. The results demonstrated that modal parameters identified from video measurement using a phase-based motion magnification technique are in good agreement with vibration measurement results using laser Doppler vibrometer. This proves that the vision-based measurements by the video camera are promising for capturing the ambient vibration of a structure. In the future, the technique can be extended to identifying deflection shapes of flexible structures whose vibration is characterized by multi vibration modes.

Acknowledgments

This research is supported by Kajima Foundation through a research grant (PI: Dionysius Siringoringo). The first author is grateful to the Japan Society for the Promotion of Science (JSPS) support for the postdoctoral fellowship program in Japan during this research work. Support of measurement device from Bridge and Structure Laboratory, The University of Tokyo is greatly acknowledged.

References

Bhowmick, S. and Nagarajaiah, S. (2020), "Identification of full-field dynamic modes using continuous displacement response estimated from vibrating edge video", *J. Sound Vib.*, 115657. https://doi.org/10.1016/j.jsv.2020.115657

Brincker, R. and Ventura, C. (2015), *Introduction to Operational Modal Analysis*, John Wiley and Sons.

Chen, J.G., Wadhwa, N., Cha, Y.J., Durand, F., Freeman, W.T. and Buyukozturk, O. (2015), "Modal identification of simple structures with high-speed video using motion magnification", *J. Sound Vib.*, **345**, 58-71. https://doi.org/10.1016/j.jsv.2015.01.024

Chen, J.G., Davis, A., Wadhwa, N., Durand, F., Freeman, W.T. and Büyüköztürk, O. (2017), "Video camera–based vibration measurement for civil infrastructure applications", *J. Infra.*

Syst., **23**(3), B4016013. https://doi.org/10.1061/(ASCE)IS.1943-555X.0000348

Chen, J.G., Adams, T.M., Sun, H., Bell, E.S. and Büyüköztürk, O. (2018), "Camera-based vibration measurement of the world war I memorial bridge in portsmouth, New Hampshire", *J. Struct. Eng*., **144**(11), 04018207. https://doi.org/10.1061/(ASCE)ST.1943-541X.0002203

Cole Jr, H.A. (1973), "On-line failure detection and damping measurement of aerospace structures by random decrement signatures", Technical Report: NASA-CR-2205, Washington, USA. https://ntrs.nasa.gov/search.jsp?R=19730010202

Feng, D. and Feng, M.Q. (2018), "Computer vision for SHM of civil infrastructure: From dynamic response measurement to damage detection–A review", *Eng. Struct*., **156**, 105-117. https://doi.org/10.1016/j.engstruct.2017.11.018

Helfrick, M.N., Niezrecki, C., Avitabile, P. and Schmidt, T. (2011), "3D digital image correlation methods for full-field vibration measurement", *Mech. Syst. Signal Proc*., **25**(3), 917-927. https://doi.org/10.1016/j.ymssp.2010.08.013

Ibrahim, S.R. (1977), "Random decrement technique for modal identification of structures", *J. Spacecr. Rockets*, **14**(11), 696-700. https://doi.org/10.2514/3.57251

Izuno, K., Tsushima, Y., Iida, T. and Kawano, K. (2008), "Dynamic response of highway bridge-lighting pole system for level 1 earthquake", *J. Appl. Mech*., **11**, 1039-1046. [In Japanese]

Molina-Viedma, A.J., Felipe-Sesé, L., López-Alba, E. and Díaz, F. (2018), "High frequency mode shapes characterization using Digital Image Correlation and phase-based motion magnification", *Mech. Syst. Signal Proc*., **102**, 245-261. https://doi.org/10.1016/j.ymssp.2017.09.019

Ni, Y.Q., Wang, Y.W., Liao, W.Y. and Chen, W.H. (2019), "A vision-based system for long-distance remote monitoring of dynamic displacement: Experimental verification on a supertall structure", *Smart. Struct. Syst*., *Int. J*., **24**(6), 769-781. https://doi.org/10.12989/sss.2019.24.6.769

Otsu, N. (1979), "A threshold selection method from gray-level histograms", *IEEE Trans. Syst*., *Man*, *Cyber*., **9**(1), 62-66. https://doi.org/10.1109/TSMC.1979.4310076

Pedrini, G., Osten, W. and Gusev, M.E. (2006), "High-speed digital holographic interferometry for vibration measurement", *Appl. Optics*, **45**(15), 3456-3462. https://doi.org/10.1364/AO.45.003456

Peeters, B. and De Roeck, G. (2001), "Stochastic system identification for operational modal analysis: a review", *J. Dyn. Syst. Measure*, *Control*, **123**(4), 659-667. https://doi.org/10.1115/1.1410370

Poozesh, P., Sarrafi, A., Mao, Z., Avitabile, P. and Niezrecki, C. (2017), "Feasibility of extracting operating shapes using phase-based motion magnification technique and stereo-photogrammetry", *J. Sound Vib*., **407**, 350-366. https://doi.org/10.1016/j.jsv.2017.06.003

Portilla, J. and Simoncelli, E.P. (2000), "A parametric texture model based on joint statistics of complex wavelet coefficients", *Int. J. Comput. Vision*, **40**(1), 49-70. https://doi.org/10.1023/A:1026553619983

Sarrafi, A., Mao, Z., Niezrecki, C. and Poozesh, P. (2018), "Vibration-based damage detection in wind turbine blades using Phase-based Motion Estimation and motion magnification", *J. Sound Vib*., **421**, 300-318. https://doi.org/10.1016/j.jsv.2018.01.050

Siringoringo, D.M. and Fujino, Y. (2006), "Experimental study of laser Doppler vibrometer and ambient vibration for vibration-based damage detection", *Eng. Struct*., **28**(13), 1803-1815 https://doi.org/10.1016/j.engstruct.2006.03.006

Siringoringo, D.M. and Fujino, Y. (2008), "System identification of suspension bridge from ambient vibration response", *Eng. Struct*., 30(2), 462-477. https://doi.org/10.1016/j.engstruct.2007.03.004

Siringoringo, D.M. and Fujino, Y. (2009), "Non-contact operational modal analysis of structural members by laser Doppler vibrometer", *Compt. Aided Civil. Infra. Eng*., **24**(4), 249-265. https://doi.org/10.1111/j.1467-8667.2008.00585.x

Siringoringo, D.M., Fujino, Y., Nagasaki, A. and Matsubara, T. (2020), "Seismic performance evaluation of existing light poles on elevated highway bridges", *Struct. Infra. Eng*., 1-15. https://doi.org/10.1080/15732479.2020.1760894

Vandiver, J.K., Dunwoody, A.B., Campbell, R.B. and Cook, M.F. (1982), "A mathematical basis for the random decrement vibration signature analysis technique", *J. Mech. Des*., **104**(2), 307-313. https://doi.org/10.1115/1.3256341

Wadhwa, N., Rubinstein, M., Durand, F. and Freeman, W.T. (2013), "Phase-based video motion processing", *ACM Trans. Graphics*, **32**(4), 1-10. https://doi.org/10.1145/2461912.2461966

Wenzel, H. (2009), *Ambient Vibration Monitoring*, John Wiley and Sons.

Yang, Y., Dorn, C., Mancini, T., Talken, Z., Kenyon, G., Farrar, C. and Mascareñas, D. (2017), "Blind identification of full-field vibration modes from video measurements with phase-based video motion magnification", *Mech. Syst. Signal Proc*., **85**, 567-590. https://doi.org/10.1016/j.ymssp.2016.08.041

Yang, Y., Dorn, C., Mancini, T., Talken, Z., Theiler, J., Kenyon, G., Farrar, C. and Mascarenas, D. (2018), "Reference-free detection of minute, non-visible, damage using full-field, high-resolution mode shapes output-only identified from digital videos of structures", *Struct. Health Monit*., **17**(3), 514-531. https://doi.org/10.1177/1475921717704385

Yang, Y., Sanchez, L., Zhang, H., Roeder, A., Bowlan, J., Crochet, J., Farrar, C. and Mascareñas, D. (2019), "Estimation of full-field, full-order experimental modal model of cable vibration from digital video measurements with physics-guided unsupervised machine learning and computer vision", *Struct. Control. Health Monitor*., **26**(6), e2358. https://doi.org/10.1002/stc.2358

Yang, Y., Dorn, C., Farrar, C. and Mascareñas, D. (2020), "Blind, simultaneous identification of full-field vibration modes and large rigid-body motion of output-only structures from digital video measurements", *Eng. Struct*., **207**, 110183. https://doi.org/10.1016/j.engstruct.2020.110183

Ye, X.W., Dong, C.Z. and Liu, T. (2016a), "Image-based structural dynamic displacement measurement using different multi-object tracking algorithms", *Smart. Struct. Syst*., *Int. J*., **17**(6), 935-956. https://doi.org/10.12989/sss.2016.17.6.935

Ye, X.W., Dong, C.Z. and Liu, T. (2016b), "Force monitoring of steel cables using vision-based sensing technology: methodology and experimental verification", *Smart. Struct. Syst*., *Int. J*., **18**(3), 585-599. https://doi.org/10.12989/sss.2016.18.3.585